Supplement of Atmos. Chem. Phys., 22, 3693–3711, 2022
https://doi.org/10.5194/acp-22-3693-2022-supplement

Atmospheric Chemistry and Physics Open Access

Supplement of

OH-initiated atmospheric degradation of hydroxyalkyl hydroperoxides: mechanism, kinetics, and structure–activity relationship

Long Chen et al.

Correspondence to: Yu Huang (huangyu@ieecas.cn)

Contents:

Figure S6. Geometries of all the stationary points for the initial reaction of $HOCH_2OOH$ with OH radical optimized at the M06-2X/6-311+G(2df,2p) level of theory

Figure S7. Geometries of all the stationary points for the initial reaction of $HOCH(CH_3)OOH$ with OH radical optimized at the M06-2X/6-311+G(2df,2p) level of theory

Figure S8. Geometries of all the stationary points for the initial reaction of $HOC(CH_3)_2OOH$ with OH radical optimized at the M06-2X/6-311+G(2df,2p) level of theory

Figure S9. Plots of the rate coefficients of every elementary pathway versus temperature in the initial reaction of $HOCH_2OOH$ with OH radical

Figure 10. Plots of the rate coefficients of every elementary pathway versus temperature in the initial reaction of $HOCH(CH_3)OOH$ with OH radical

Figure S11. Plots of the rate coefficients of every elementary pathway versus temperature in the initial reaction of $HOC(CH_3)_2OOH$ with OH radical

Figure S12. Plots of the rate coefficients of R31, R32 and R33 versus temperature

Figure S13. PES ($\Delta G_a^{\#}$ and $\Delta E_a^{\#}$, in italics) for the isomerization of $HOCH_3CHOO$ radical predicted at the M06-2X/ma-TZVP//M06-2X/6-311+G(2df,2p) level of theory

Figure S14. PES ($\Delta G_a^{\#}$ and $\Delta E_a^{\#}$, in italics) for the isomerization of $HO(CH_3)_2COO$ radical predicted at the M06-2X/ma-TZVP//M06-2X/6-311+G(2df,2p) level of theory

Table S1 Y//X (Y = M06-2X, CCSD(T), X = 6-311+G(2df,2p), ma-TZVP) calculated energy barrier ($\Delta E_a^{\#}$, $\Delta G_a^{\#}$) for ·OH + HHPs reactions based on the M06-2X/6-311+G(2df,2p) optimized geometries (kcal·mol^{-1})

Entry	CCSD(T)/6-311+G(2df,2p)		ma-TZVP	
	$\Delta E_a^{\#}$	$\Delta G_a^{\#}$	$\Delta E_a^{\#}$	$\Delta G_a^{\#}$
$HOCH_2OOH$ + ·OH				
R1(O_1-H_1)	6.0	6.4	6.1	6.4
R2(C_1-H_3)	4.4	5.6	4.6	5.8
R3(C_1-H_4)	4.8	4.5	5.3	5.4
R4(O_3-H_2)	1.1	2.1	0.5	1.5
$HOCH(CH_3)OOH$ + ·OH				
R5(O_1-H_1)	6.5	7.1	6.5	7.2
R6(C_1-H_3)	0.5	1.4	1.3	2.2
R7-1(C_2-H_4)	5.2	6.5	5.6	6.9
R7-2(C_2-H_5)	6.1	6.9	6.5	7.4
R7-3(C_2-H_6)	5.7	6.4	6.7	7.4
R8(O_3-H_2)	0.7	2.0	0.7	1.7
$HOC(CH_3)_2OOH$ + ·OH				
R9(O_1-H_1)	6.4	7.0	6.7	7.4
R10-1(C_2-H_3)	5.2	5.9	5.1	5.8
R10-2(C_2-H_4)	5.1	6.0	5.8	6.6
R10-3(C_2-H_5)	5.2	6.1	5.8	6.8
R11-1(C_3-H_6)	5.9	6.4	6.5	7.0
R11-2(C_3-H_7)	5.1	5.8	6.3	6.9
R11-3(C_3-H_8)	5.9	7.1	5.8	6.0
R12(O_3-H_2)	2.7	2.8	2.5	2.7

Table S2 Rate coefficients (cm^3 $molecule^{-1}$ s^{-1}) of every elementary pathway involved in the initial reaction of $HOCH_2OOH$ with OH radical computed at different temperatures

T/K	$k_{R1(O1-H1)}$	$k_{R2(C1-H3)}$	$k_{R3(C1-H4)}$	$k_{R4(O3-H2)}$	k_{tot}
273	2.9×10^{-13}	1.4×10^{-12}	2.2×10^{-12}	4.5×10^{-11}	4.9×10^{-11}
280	2.3×10^{-13}	1.2×10^{-12}	2.1×10^{-12}	3.6×10^{-11}	3.0×10^{-11}
298	1.8×10^{-13}	9.9×10^{-13}	2.0×10^{-12}	2.9×10^{-11}	3.3×10^{-11}
300	1.5×10^{-13}	8.6×10^{-13}	1.9×10^{-12}	2.4×10^{-11}	2.7×10^{-11}
320	1.1×10^{-13}	6.7×10^{-13}	1.8×10^{-12}	1.7×10^{-11}	2.0×10^{-11}
340	8.6×10^{-14}	5.5×10^{-13}	1.8×10^{-12}	1.3×10^{-11}	1.6×10^{-11}
360	7.2×10^{-14}	4.6×10^{-13}	1.7×10^{-12}	1.0×10^{-11}	1.3×10^{-11}
380	6.2×10^{-14}	4.1×10^{-13}	1.7×10^{-12}	8.2×10^{-12}	1.0×10^{-11}
400	5.6×10^{-14}	3.6×10^{-13}	1.7×10^{-12}	6.8×10^{-12}	8.9×10^{-12}

Table S3 Rate coefficients (cm^3 $molecule^{-1}$ s^{-1}) of every elementary pathway involved in the initial reaction of $HOCH(CH_3)OOH$ with OH radical computed at different temperatures

T/K	$k_{R5(O1-H1)}$	$k_{R6(C1-H3)}$	$k_{R7-1(C2-H4)}$	$k_{R7-2(C2-H5)}$
273	3.8×10^{-13}	1.1×10^{-12}	5.8×10^{-13}	6.6×10^{-13}
280	2.9×10^{-13}	1.0×10^{-12}	5.3×10^{-13}	5.5×10^{-13}
298	2.3×10^{-13}	9.5×10^{-13}	4.7×10^{-13}	4.8×10^{-13}
300	1.9×10^{-13}	9.0×10^{-13}	4.2×10^{-13}	4.2×10^{-13}
320	1.3×10^{-13}	8.3×10^{-13}	3.8×10^{-13}	3.5×10^{-13}
340	1.0×10^{-13}	7.7×10^{-13}	3.3×10^{-13}	3.1×10^{-13}
360	8.2×10^{-14}	7.4×10^{-13}	3.2×10^{-13}	2.8×10^{-13}
380	7.0×10^{-14}	7.1×10^{-13}	2.9×10^{-13}	2.7×10^{-13}
400	6.2×10^{-14}	6.9×10^{-13}	2.8×10^{-13}	2.6×10^{-13}

T/K	$k_{R7-3(C2-H6)}$	$k_{R8(O3-H2)}$	k'_{tot}
273	7.3×10^{-13}	4.2×10^{-11}	4.5×10^{-11}
280	6.1×10^{-13}	3.4×10^{-11}	3.7×10^{-11}
298	5.2×10^{-13}	2.8×10^{-11}	3.0×10^{-11}
300	4.7×10^{-13}	2.3×10^{-11}	2.5×10^{-11}
320	3.9×10^{-13}	1.7×10^{-11}	1.9×10^{-11}
340	3.4×10^{-13}	1.3×10^{-11}	1.4×10^{-11}
360	3.1×10^{-13}	9.8×10^{-12}	1.2×10^{-11}
380	2.9×10^{-13}	7.9×10^{-12}	9.5×10^{-12}
400	2.8×10^{-13}	6.6×10^{-12}	8.1×10^{-12}

Table S4 Rate coefficients (cm^3 $molecule^{-1}$ s^{-1}) of every elementary pathway involved in the initial reaction of $HOC(CH_3)_2OOH$ with OH radical computed at different temperatures

T/K	$k_{R9(O1\text{-}H1)}$	$k_{R10\text{-}1(C2\text{-}H3)}$	$k_{R10\text{-}2(C2\text{-}H4)}$	$k_{R10\text{-}3(C2\text{-}H5)}$
273	2.5×10^{-13}	4.6×10^{-13}	9.7×10^{-13}	8.9×10^{-13}
280	1.9×10^{-13}	3.7×10^{-13}	9.4×10^{-13}	7.4×10^{-13}
298	1.5×10^{-13}	3.1×10^{-13}	8.2×10^{-13}	6.4×10^{-13}
300	1.2×10^{-13}	2.6×10^{-13}	7.1×10^{-13}	5.6×10^{-13}
320	8.5×10^{-14}	2.0×10^{-13}	5.6×10^{-13}	4.5×10^{-13}
340	6.4×10^{-14}	1.6×10^{-13}	4.6×10^{-13}	3.8×10^{-13}
360	5.2×10^{-14}	1.3×10^{-13}	4.0×10^{-13}	3.4×10^{-13}
380	4.4×10^{-14}	1.1×10^{-13}	3.6×10^{-13}	3.1×10^{-13}
400	3.8×10^{-14}	1.0×10^{-13}	3.2×10^{-13}	2.8×10^{-13}

T/K	$k_{R11\text{-}1(C3\text{-}H6)}$	$k_{R11\text{-}2(C3\text{-}H7)}$	$k_{R11\text{-}3(C3\text{-}H8)}$	$k_{R12(O3\text{-}H2)}$	k''_{tot}
273	4.9×10^{-13}	8.3×10^{-13}	5.3×10^{-13}	2.5×10^{-11}	2.9×10^{-11}
280	4.1×10^{-13}	6.9×10^{-13}	4.0×10^{-13}	1.8×10^{-11}	2.1×10^{-11}
298	3.5×10^{-13}	5.9×10^{-13}	3.2×10^{-13}	1.3×10^{-11}	1.6×10^{-11}
300	3.1×10^{-13}	5.2×10^{-13}	2.6×10^{-13}	9.9×10^{-12}	1.3×10^{-11}
320	2.5×10^{-13}	4.2×10^{-13}	1.8×10^{-13}	6.0×10^{-12}	8.2×10^{-12}
340	2.1×10^{-13}	3.6×10^{-13}	1.3×10^{-13}	4.0×10^{-12}	5.7×10^{-12}
360	1.9×10^{-13}	3.3×10^{-13}	1.0×10^{-13}	2.7×10^{-12}	4.3×10^{-12}
380	1.8×10^{-13}	2.9×10^{-13}	8.3×10^{-14}	2.0×10^{-12}	3.4×10^{-12}
400	1.6×10^{-13}	2.7×10^{-13}	6.9×10^{-14}	1.5×10^{-12}	2.8×10^{-12}

Table S5 Rate coefficients (cm^3 $molecule^{-1}$ s^{-1}) of HO_2 radical reactions with $HOCH_2OO$ (R31), $HOCH(CH_3)OO$ (R32) and $HO(CH_3)_2COO$ radicals (R33) computed at different temperatures

T/K	k_{R31}	k_{R32}	k_{R33}
273	3.1×10^{-11}	9.1×10^{-11}	1.5×10^{-10}
280	2.3×10^{-11}	6.4×10^{-11}	1.0×10^{-10}
298	1.7×10^{-11}	4.6×10^{-11}	7.4×10^{-11}
300	1.3×10^{-11}	3.4×10^{-11}	5.3×10^{-11}
320	8.1×10^{-12}	2.0×10^{-11}	3.0×10^{-11}
340	5.4×10^{-12}	1.2×10^{-11}	1.8×10^{-11}
360	3.8×10^{-12}	8.3×10^{-12}	1.2×10^{-11}
380	2.8×10^{-12}	5.8×10^{-12}	8.3×10^{-12}
400	2.1×10^{-12}	4.2×10^{-12}	5.9×10^{-12}

Table S6 The relative free energy and Boltzmann populations (w_i) of the conformation of $HOCH_2OO$ radical at the M06-2X/6-311+G(2df,2p) level of theory

Conformer	ΔG(kcal mol^{-1})	w_i
$HOCH_2OO$-a	0.000	46.39%
$HOCH_2OO$-b	0.001	46.31%
$HOCH_2OO$-c	1.623	2.99%
$HOCH_2OO$-d	1.406	4.32%

Table S7 The relative free energy and Boltzmann populations (w_i) of the conformation of $HOCH(CH_3)OO$ radical at the M06-2X/6-311+G(2df,2p) level of theory

Conformer	ΔG(kcal mol^{-1})	w_i
$HOCH(CH_3)OO$-a	0.000	80.13%
$HOCH(CH_3)OO$-b	0.942	16.33%
$HOCH(CH_3)OO$-c	2.218	1.89%
$HOCH(CH_3)OO$-d	2.299	1.65%

Table S8 The relative free energy and Boltzmann populations (w_i) of the conformation of $HO(CH_3)_2COO$ radical at the M06-2X/6-311+G(2df,2p) level of theory

Conformer	ΔG(kcal·mol^{-1})	w_i
$HO(CH_3)_2COO$-a	0.000	88.04%
$HO(CH_3)_2COO$-b	1.334	9.25%
$HO(CH_3)_2COO$-c	2.062	2.71%

Table S9 The single-conformer rate coefficients ($k_{IRC\text{-}TST}$) and multi-conformer rate coefficients ($k_{MC\text{-}TST}$) of $HOCH_2OO$ radical isomerization computed at different temperatures

T/K	$k_{IRC\text{-}TST}$(TS22-a)	$k_{IRC\text{-}TST}$(TS22-b1)	$k_{IRC\text{-}TST}$(TS22-b2)	$k_{MC\text{-}TST}$
273	1.9×10^{-17}	2.1×10^{-17}	6.6×10^{-20}	1.8×10^{-17}
280	9.5×10^{-17}	1.0×10^{-16}	3.8×10^{-19}	9.1×10^{-17}
298	4.6×10^{-16}	4.8×10^{-16}	2.1×10^{-18}	4.4×10^{-16}
300	2.2×10^{-15}	2.3×10^{-15}	1.1×10^{-17}	2.0×10^{-15}
320	4.3×10^{-14}	4.4×10^{-14}	2.7×10^{-16}	4.1×10^{-14}
340	7.6×10^{-13}	7.7×10^{-13}	6.0×10^{-15}	7.1×10^{-13}
360	1.2×10^{-11}	1.2×10^{-11}	1.1×10^{-13}	1.1×10^{-11}
380	1.5×10^{-10}	1.5×10^{-10}	1.8×10^{-12}	1.4×10^{-10}
400	1.6×10^{-09}	1.6×10^{-09}	2.4×10^{-11}	1.5×10^{-09}

Table S10 The single-conformer rate coefficients ($k_{IRC\text{-}TST}$) and multi-conformer rate coefficients ($k_{MC\text{-}TST}$) of $HOCH(CH_3)OO$ radical isomerization computed at different temperatures

T/K	$k_{IRC\text{-}TST}$(TS23-a)	$k_{IRC\text{-}TST}$(TS23-b)	$k_{IRC\text{-}TST}$(TS23-c1)	$k_{IRC\text{-}TST}$(TS23-c2)	$k_{MC\text{-}TST}$
273	8.0×10^{-18}	8.3×10^{-14}	3.3×10^{-18}	1.8×10^{-13}	1.7×10^{-14}
280	4.3×10^{-17}	3.5×10^{-13}	1.5×10^{-17}	7.9×10^{-13}	7.2×10^{-14}
298	2.3×10^{-16}	1.4×10^{-12}	6.9×10^{-17}	3.3×10^{-12}	2.9×10^{-13}
300	1.2×10^{-15}	5.1×10^{-12}	3.1×10^{-16}	1.3×10^{-11}	1.1×10^{-12}
320	2.6×10^{-14}	5.8×10^{-11}	6.1×10^{-15}	1.5×10^{-10}	1.2×10^{-11}
340	5.2×10^{-13}	5.5×10^{-10}	1.1×10^{-13}	1.6×10^{-9}	1.2×10^{-10}
360	8.6×10^{-12}	4.5×10^{-09}	1.8×10^{-12}	1.3×10^{-8}	9.8×10^{-10}
380	1.2×10^{-10}	3.2×10^{-08}	2.5×10^{-11}	9.7×10^{-8}	7.1×10^{-9}
400	1.3×10^{-9}	2.0×10^{-7}	3.0×10^{-10}	6.3×10^{-7}	4.6×10^{-8}

Table S11 The single-conformer rate coefficients ($k_{IRC\text{-}TST}$) and multi-conformer rate coefficients ($k_{MC\text{-}TST}$) of $HO(CH_3)_2COO$ radical isomerization computed at different temperatures

T/K	$k_{IRC\text{-}TST}$(TS24-a)	$k_{IRC\text{-}TST}$(TS24-b1)	$k_{IRC\text{-}TST}$(TS24-b2)	$k_{IRC\text{-}TST}$(TS24-c)	$k_{MC\text{-}TST}$
273	1.4×10^{-13}	1.2×10^{-13}	2.0×10^{-14}	1.6×10^{-12}	1.8×10^{-13}
280	6.1×10^{-13}	5.7×10^{-13}	9.0×10^{-14}	6.2×10^{-12}	7.7×10^{-13}
298	2.5×10^{-12}	2.4×10^{-12}	3.9×10^{-13}	2.3×10^{-11}	3.0×10^{-12}
300	9.2×10^{-12}	9.6×10^{-12}	1.5×10^{-12}	8.0×10^{-11}	1.1×10^{-11}
320	1.1×10^{-10}	1.2×10^{-10}	2.0×10^{-11}	8.3×10^{-10}	1.3×10^{-10}
340	1.1×10^{-9}	1.3×10^{-9}	2.2×10^{-10}	7.2×10^{-9}	1.3×10^{-9}
360	8.7×10^{-9}	1.1×10^{-8}	1.9×10^{-9}	5.3×10^{-8}	1.0×10^{-8}
380	6.3×10^{-8}	8.3×10^{-8}	1.5×10^{-8}	3.5×10^{-7}	7.4×10^{-8}
400	4.1×10^{-7}	5.4×10^{-7}	1.0×10^{-7}	2.1×10^{-6}	4.7×10^{-7}

Table S12 Rate coefficients of the dominant pathways of the fragmentation of $HOCH_2O\cdot$(R41), $HOCH(CH_3)O\cdot$(R45) and $HO(CH_3)_2CO\cdot$(R51) computed at different temperatures

T/K	k_{R41} (cm^3 $molecule^{-1}$ s^{-1})	k_{R45} (s^{-1})	k_{R51} (s^{-1})
273	4.3×10^{-18}	2.0×10^{6}	2.6×10^{6}
280	5.0×10^{-18}	2.9×10^{6}	3.8×10^{6}
298	7.6×10^{-18}	7.3×10^{6}	9.5×10^{6}
300	7.9×10^{-18}	8.1×10^{6}	1.0×10^{7}
320	1.2×10^{-17}	1.9×10^{7}	2.5×10^{7}
340	1.8×10^{-17}	4.4×10^{7}	5.6×10^{7}
360	2.6×10^{-17}	9.0×10^{7}	1.1×10^{8}
380	3.7×10^{-17}	1.7×10^{8}	2.2×10^{8}
400	5.1×10^{-17}	3.1×10^{8}	3.8×10^{8}

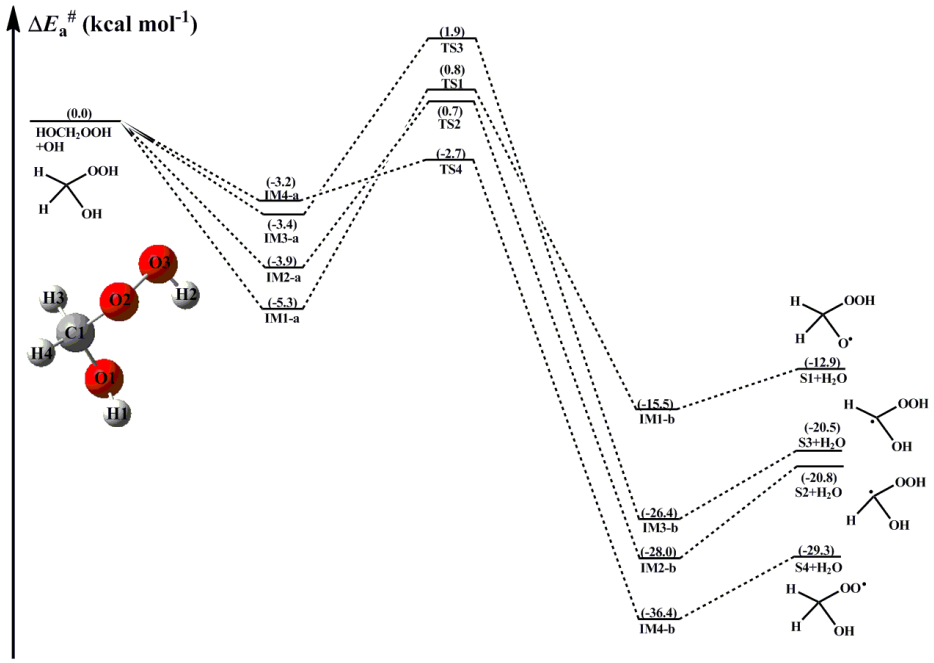

Figure S1. PES ($\Delta E_a^{\#}$) for the OH-initiated reactions of $HOCH_2OOH$ from the CH_2OO + H_2O reaction predicted at the M06-2X/ma-TZVP//M06-2X/6-311+G(2df,2p) level of theory (a and b represent the pre-reactive and post-reactive complexes)

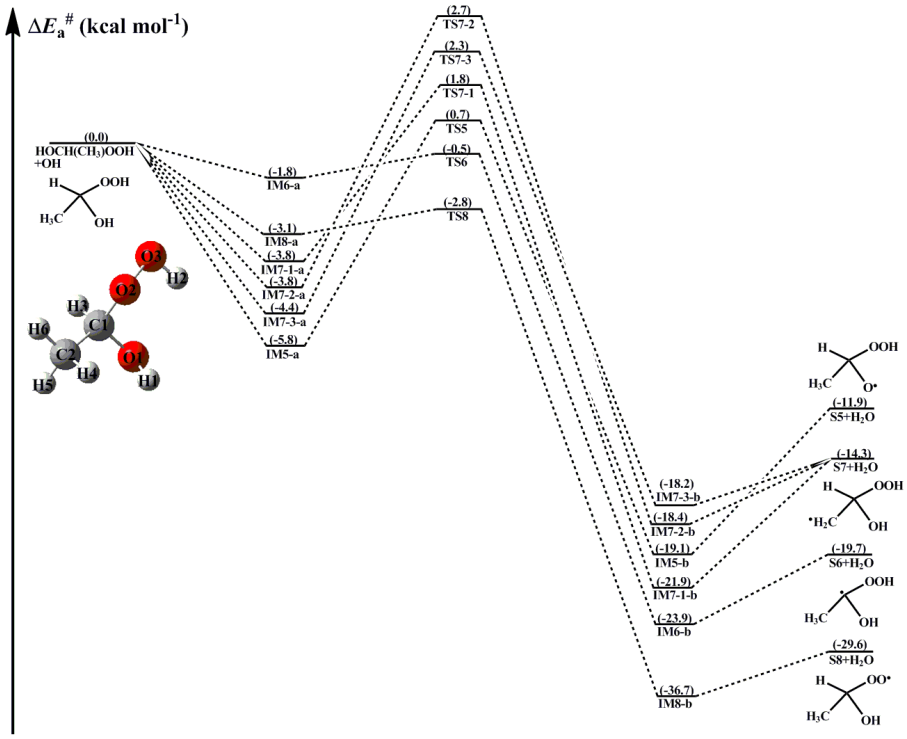

Figure S2. PES ($\Delta E_a^{\#}$) for the OH-initiated reactions of $HOCH(CH_3)OOH$ from the *anti*-CH_3CHOO + H_2O reaction predicted at the M06-2X/ma-TZVP//M06-2X/6-311+G(2df,2p) level of theory (a and b represent the pre-reactive and post-reactive complexes)

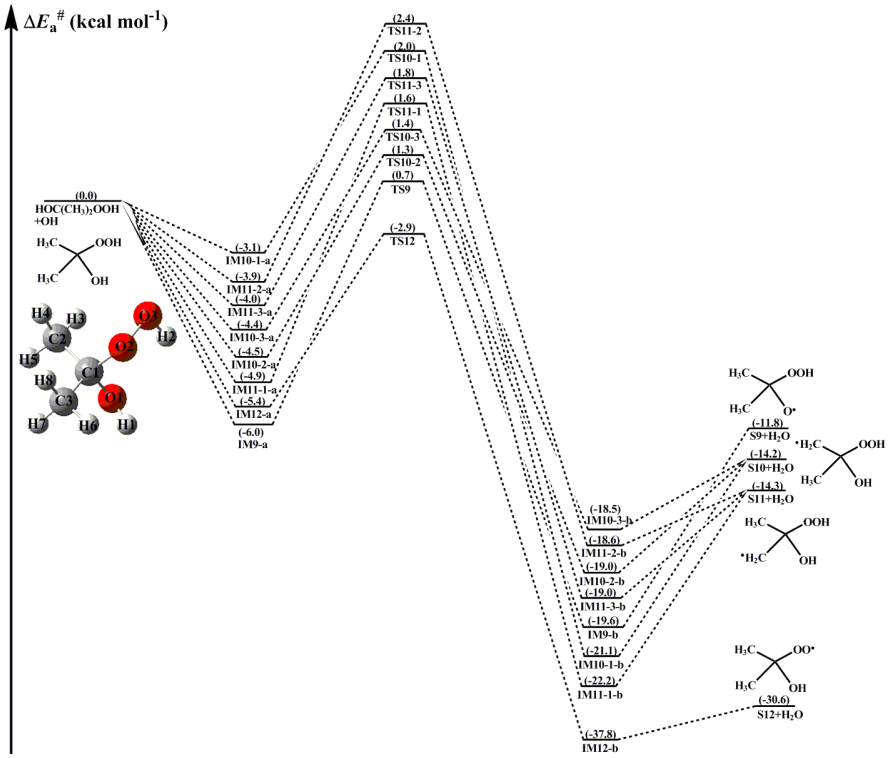

Figure S3. PES ($\Delta E_a^{\#}$) for the OH-initiated reactions of $HOC(CH_3)_2OOH$ from the $(CH_3)_2COO$ + H_2O reaction predicted at the M06-2X/ma-TZVP//M06-2X/6-311+G(2df,2p) level of theory (a and b represent the pre-reactive and post-reactive complexes)

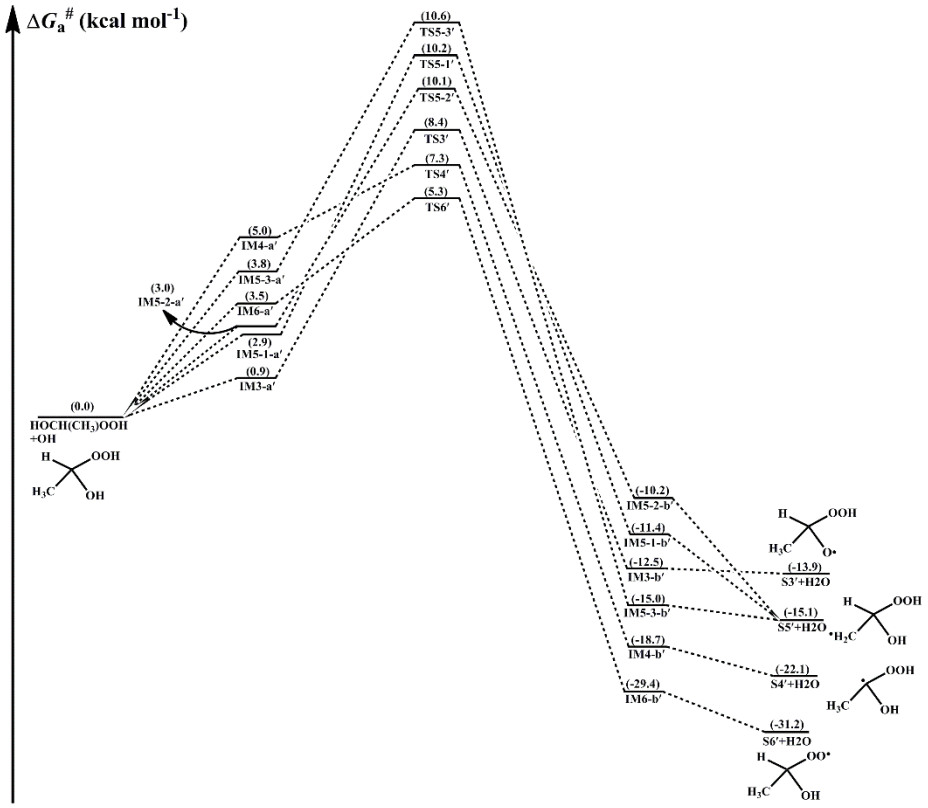

Figure S4. PES ($\Delta G_a^{\#}$) for the OH-initiated reactions of $HOCH(CH_3)OOH$ from the *syn*-CH_3CHOO + H_2O reaction predicted at the M06-2X/ma-TZVP//M06-2X/6-311+G(2df,2p) level of theory (a and b represent the pre-reactive and post-reactive complexes)

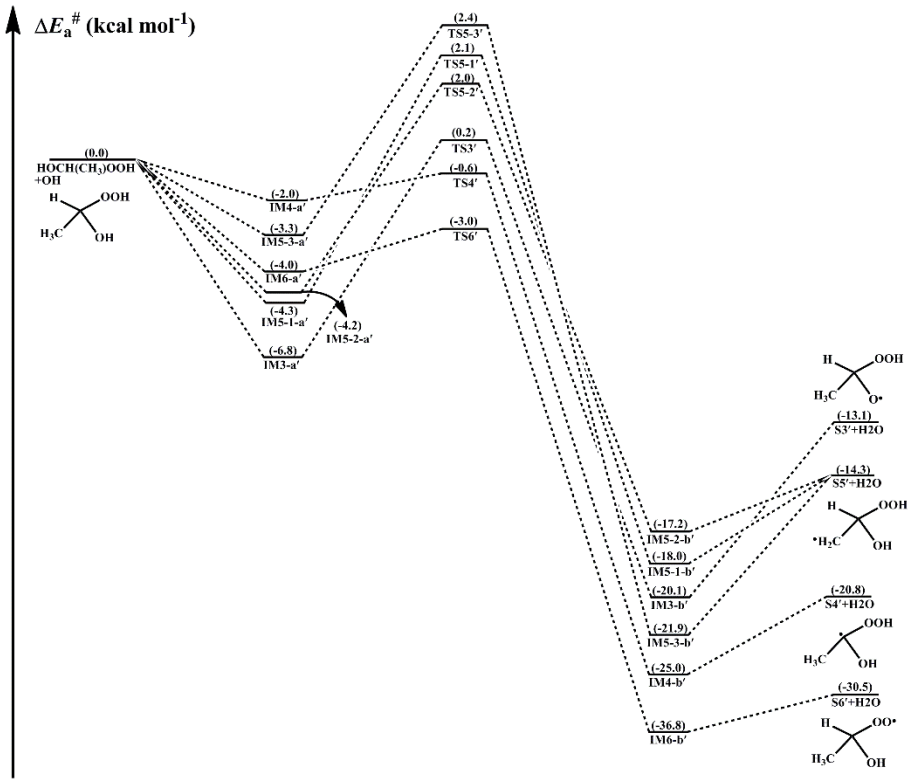

Figure S5. PES ($\Delta E_a^{\#}$) for the OH-initiated reactions of $HOCH(CH_3)OOH$ from the *syn*-CH_3CHOO + H_2O reaction predicted at the M06-2X/ma-TZVP//M06-2X/6-311+G(2df,2p) level of theory (a and b represent the pre-reactive and post-reactive complexes)

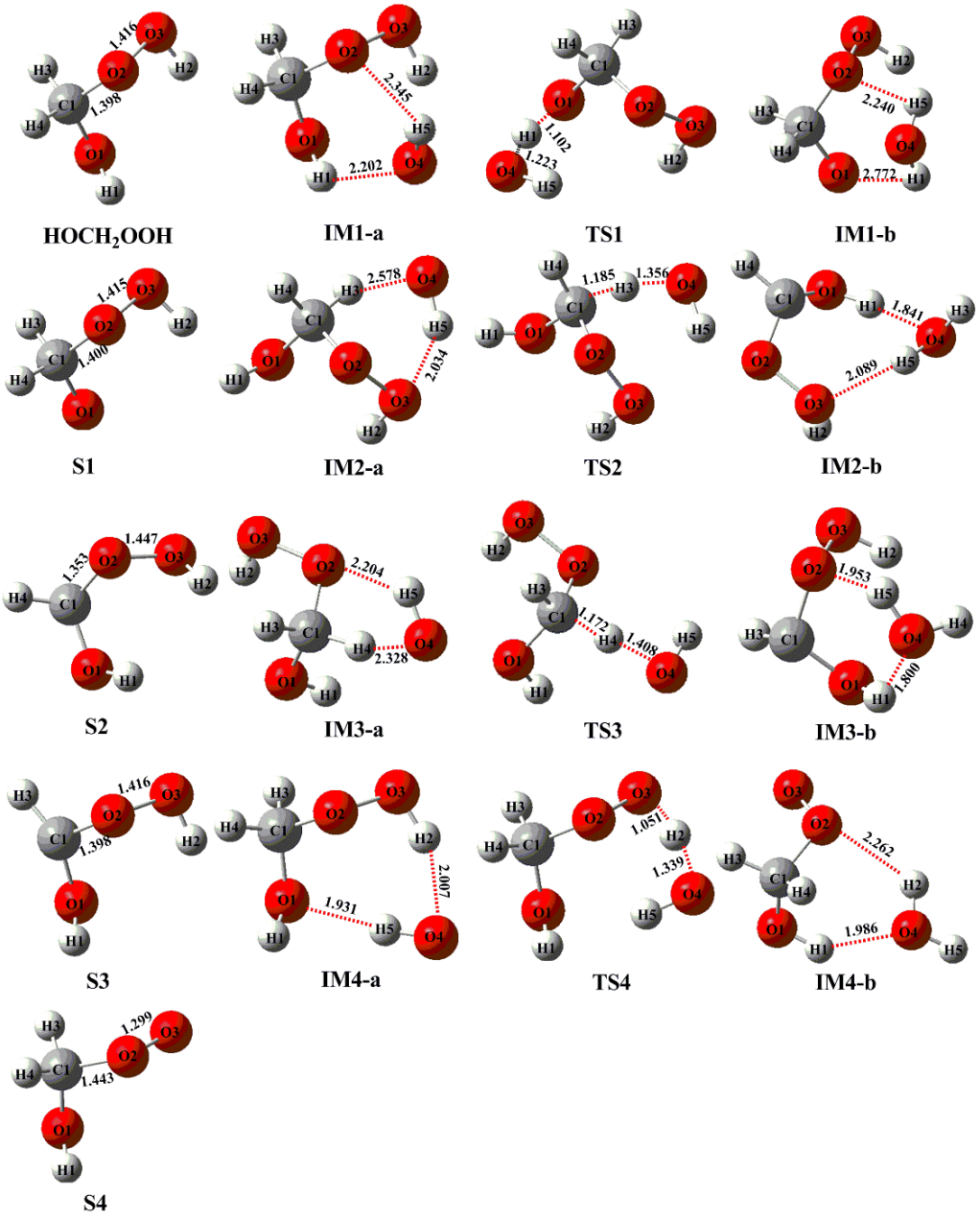

Figure S6. Geometries of all the stationary points for the initial reaction of $HOCH_2OOH$ with OH radical optimized at the M06-2X/6-311+G(2df,2p) level of theory

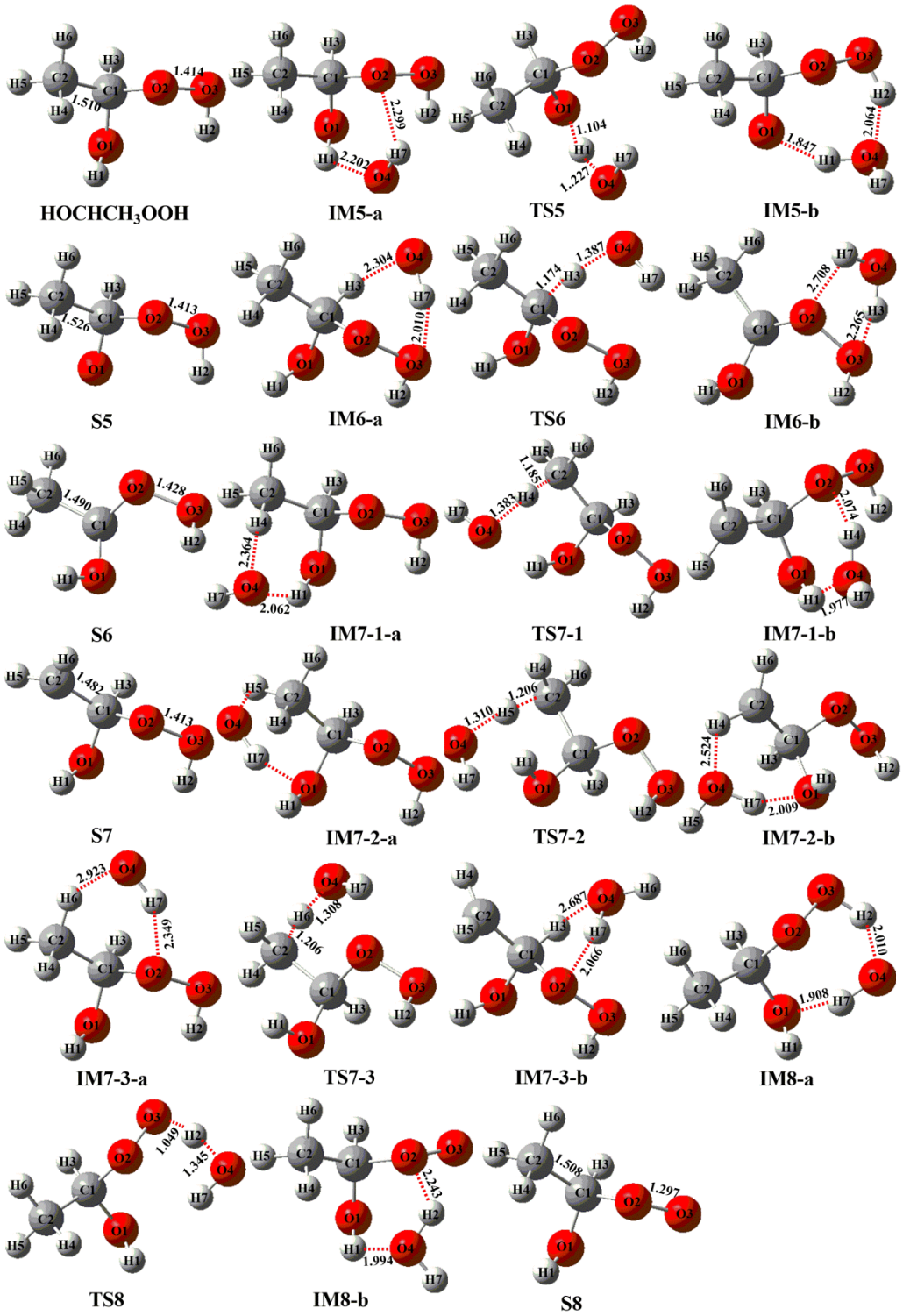

Figure S7. Geometries of all the stationary points for the initial reaction of $HOCH(CH_3)OOH$ with OH radical optimized at the M06-2X/6-311+G(2df,2p) level of theory

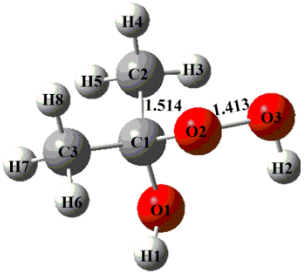

$HOC(CH_3)_2OOH$

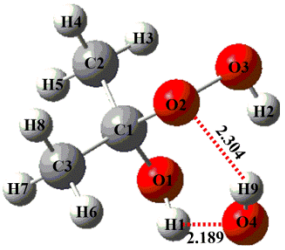

IM9-a

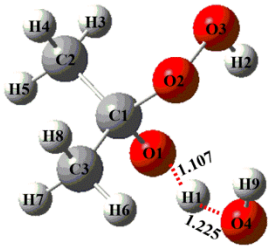

TS9

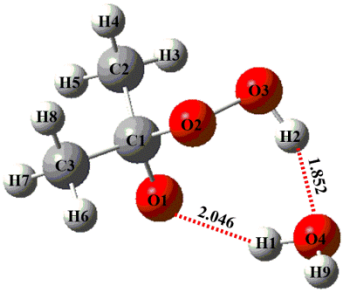

IM9-b

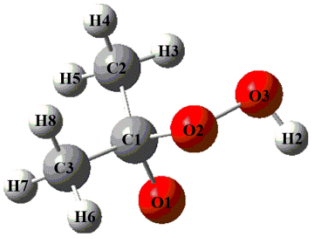

S9

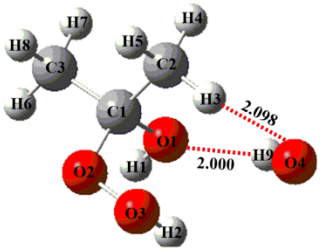

IM10-1-a

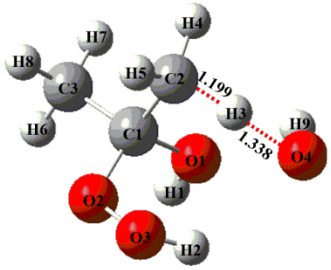

TS10-1

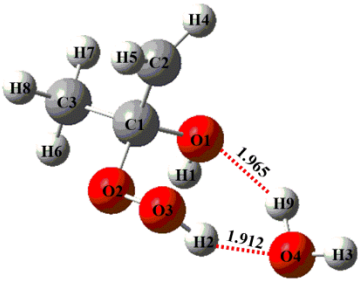

IM10-1-b

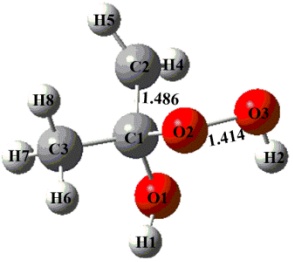

S10

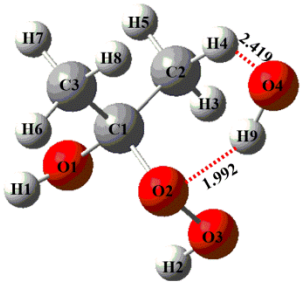

IM10-2-a

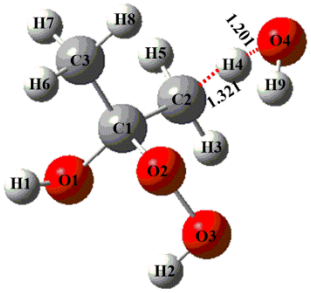

TS10-2

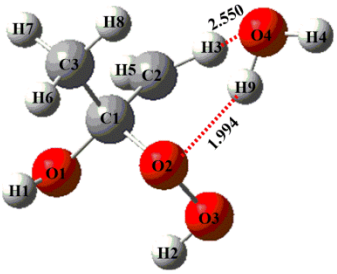

IM10-2-b

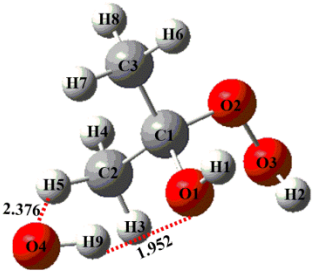

IM10-3-a

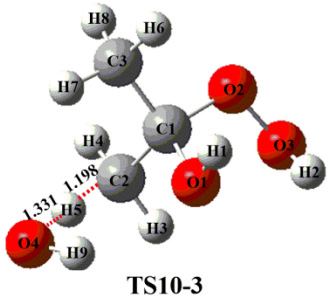

TS10-3

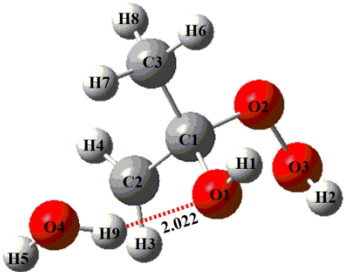

IM10-3-b

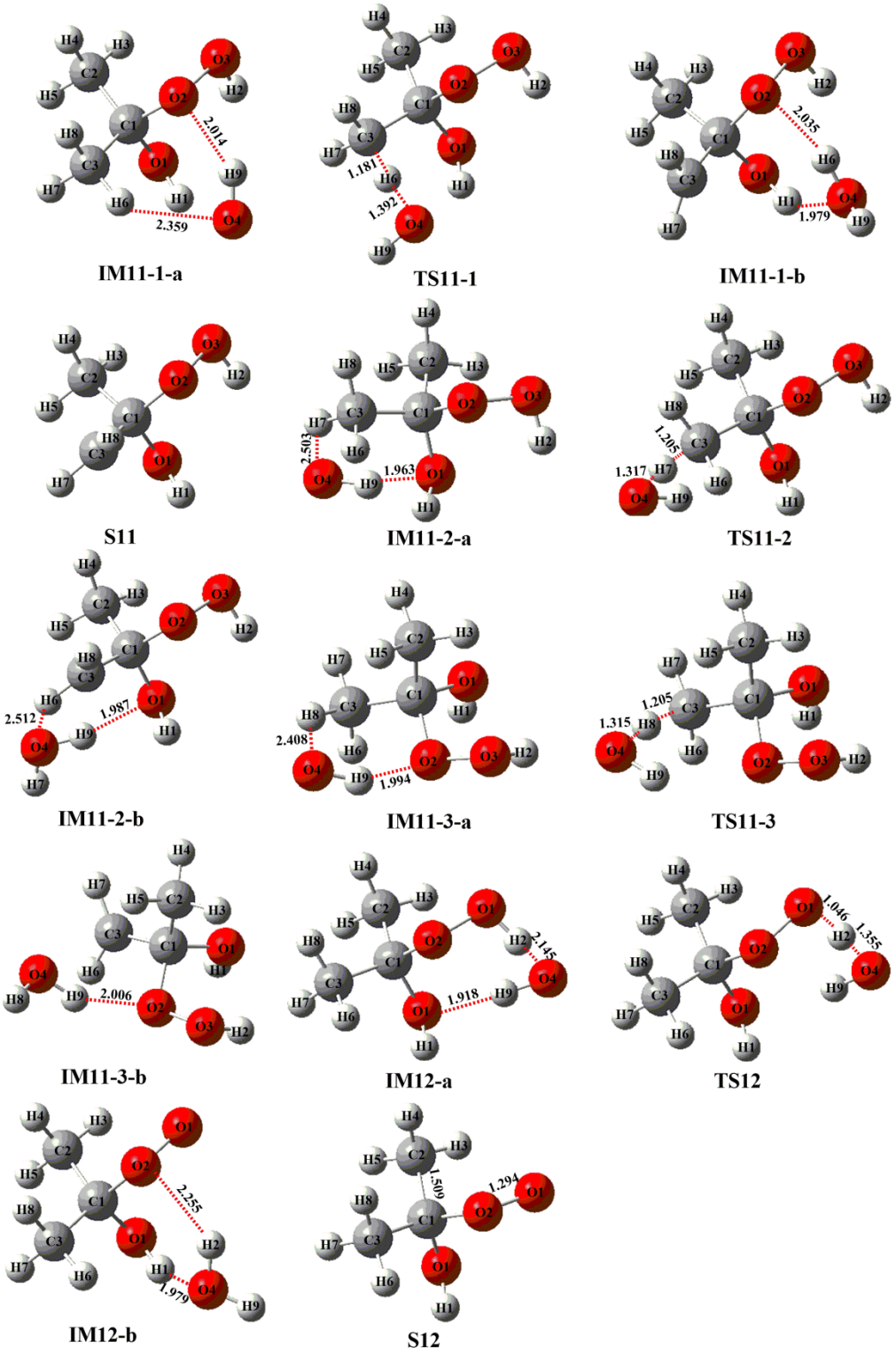

Figure S8. Geometries of all the stationary points for the initial reaction of $HOC(CH_3)_2OOH$ with OH radical optimized at the M06-2X/6-311+G(2df,2p) level of theory

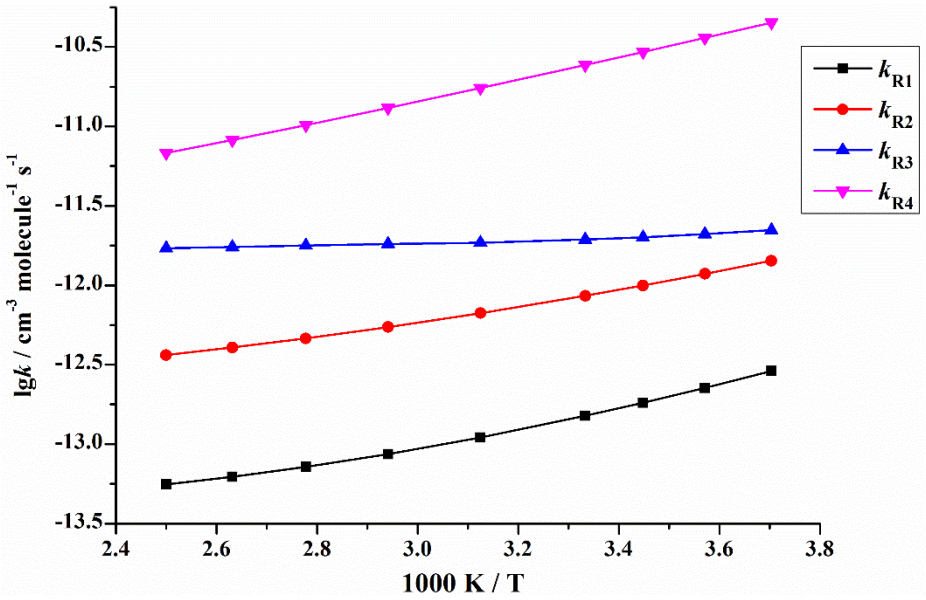

Figure S9. Plots of the rate coefficients of every elementary pathway versus temperature in the initial reaction of $HOCH_2OOH$ with OH radical

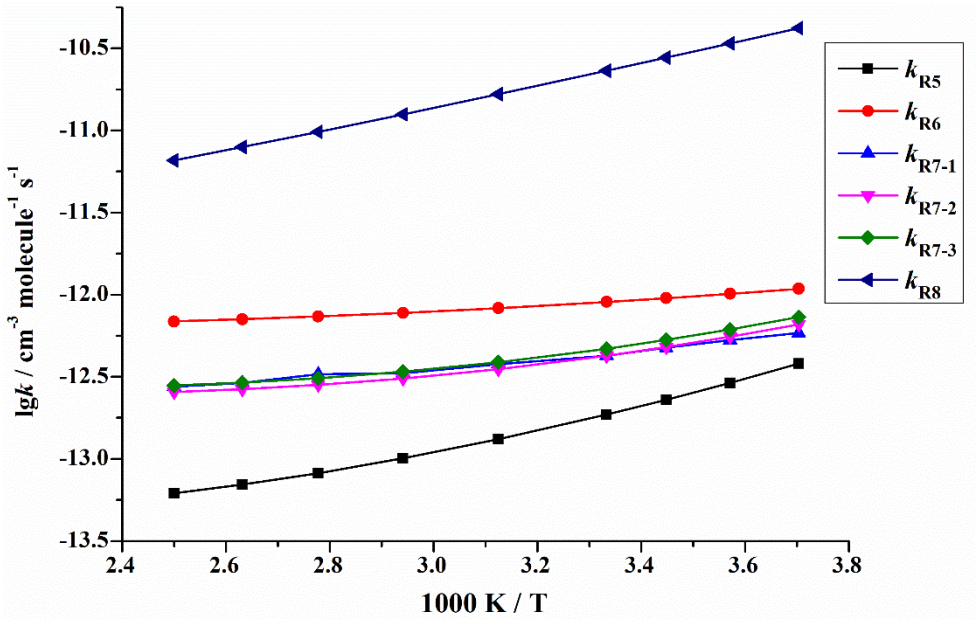

Figure 10. Plots of the rate coefficients of every elementary pathway versus temperature in the initial reaction of $HOCH(CH_3)OOH$ with OH radical

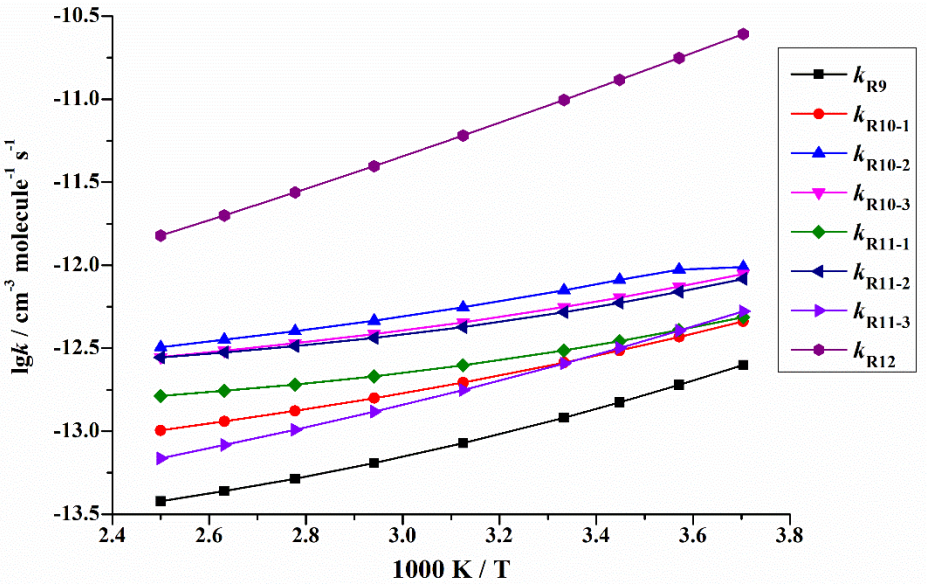

Figure S11. Plots of the rate coefficients of every elementary pathway versus temperature in the initial reaction of $HOC(CH_3)_2OOH$ with OH radical

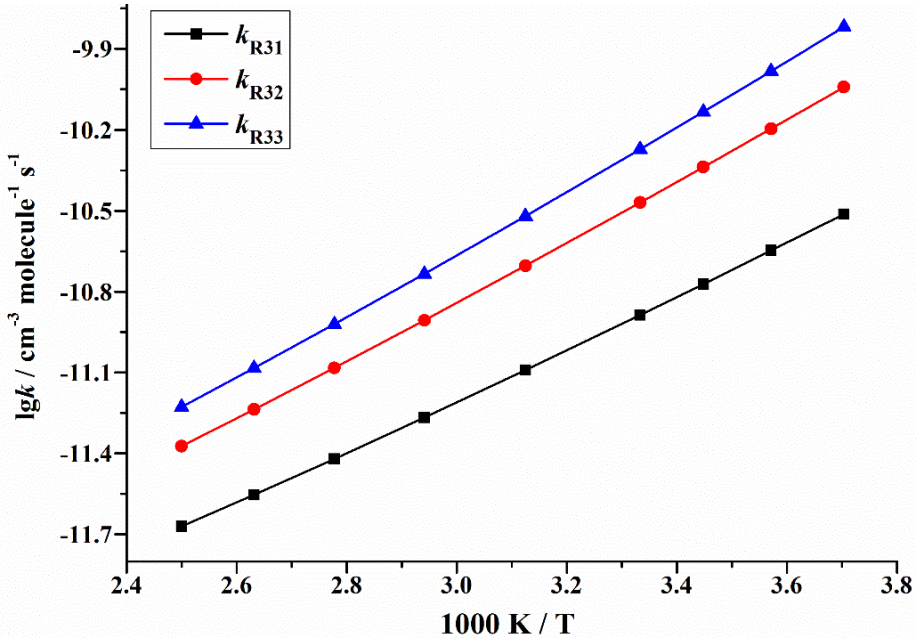

Figure S12. Plots of the rate coefficients of R31, R32 and R33 versus temperature

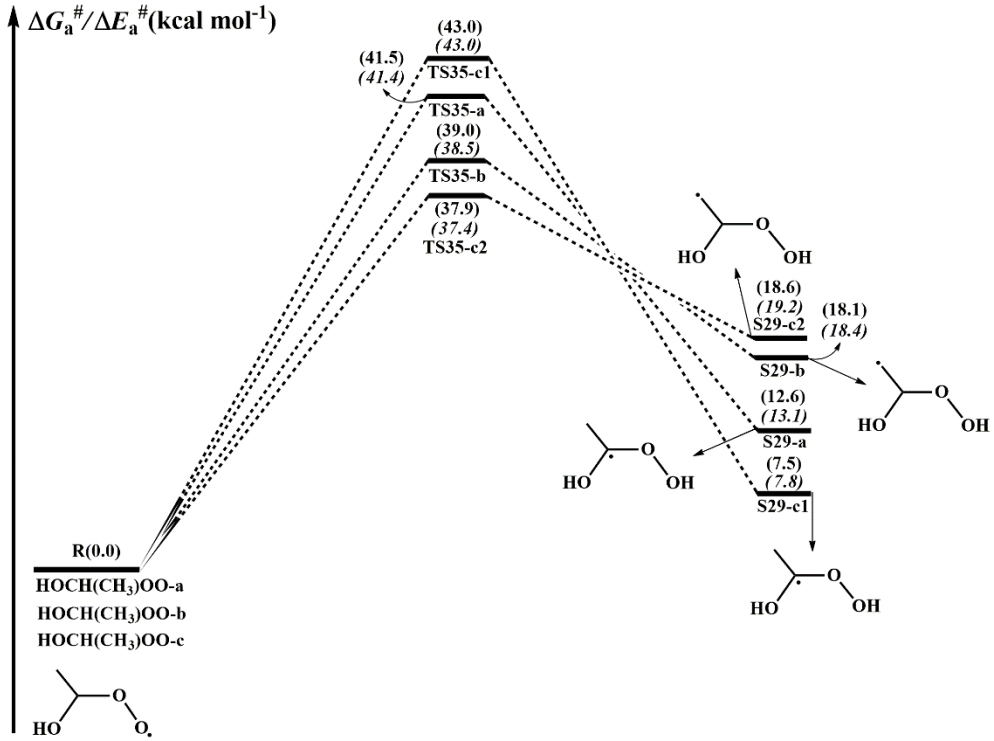

Figure S13. PES ($\Delta G_a^{\#}$ and $\Delta E_a^{\#}$, in italics) for the isomerization of $HOCH_3CHOO$ radical predicted at the M06-2X/ma-TZVP//M06-2X/6-311+G(2df,2p) level of theory

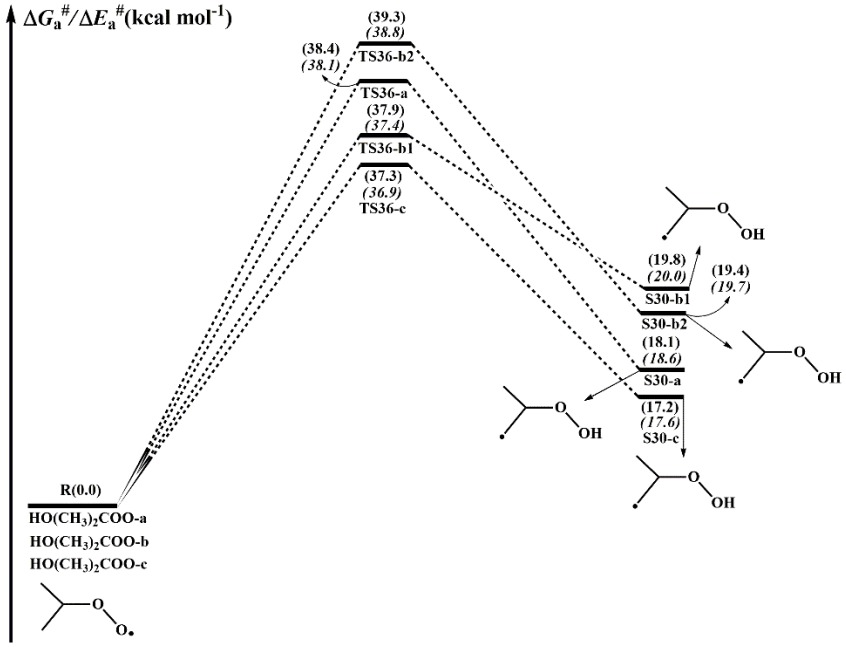

Figure S14. PES ($\Delta G_a^{\#}$ and $\Delta E_a^{\#}$, in italics) for the isomerization of $HO(CH_3)_2COO$ radical predicted at the M06-2X/ma-TZVP//M06-2X/6-311+G(2df,2p) level of theory